

# Unveiling Beamforming Strategies of Starlink LEO Satellites

Mohammad Neinavaie and Zaher M. Kassas  
*The Ohio State University*

## BIOGRAPHIES

**Mohammad Neinavaie** is a Ph.D. student at The Ohio State University and member of the Autonomous Systems Perception, Intelligence, and Navigation (ASPIN) Laboratory. He received a B.E. in electrical engineering and an M.S. in digital communication systems from Shiraz University. His research interests include opportunistic navigation, blind opportunistic navigation, cognitive radio, wireless communication systems, and software-defined radio.

**Zaher (Zak) M. Kassas** is a Professor at The Ohio State University and director of the Autonomous Systems Perception, Intelligence, and Navigation (ASPIN) Laboratory. He is also director of the U.S. Department of Transportation Center: CARMEN (Center for Automated Vehicle Research with Multimodal AssurEd Navigation), focusing on navigation resiliency and security of highly automated transportation systems. He received a B.E. in Electrical Engineering from the Lebanese American University, an M.S. in Electrical and Computer Engineering from The Ohio State University, and an M.S.E. in Aerospace Engineering and a Ph.D. in Electrical and Computer Engineering from The University of Texas at Austin. He is a recipient of the 2018 National Science Foundation (NSF) CAREER award, 2019 Office of Naval Research (ONR) Young Investigator Program (YIP) award, 2022 Air Force Office of Scientific Research (AFOSR) YIP award, 2018 IEEE Walter Fried Award, 2018 Institute of Navigation (ION) Samuel Burka Award, and 2019 ION Col. Thomas Thurlow Award. His research interests include cyber-physical systems, navigation systems, autonomous vehicles, and intelligent transportation systems.

## ABSTRACT

This paper studies the beamforming strategies of multiple-input multiple-output (MIMO) Starlink low Earth orbit (LEO) satellites. Applying a maximum likelihood (ML) estimation framework to the signal-to-noise ratio (SNR), the beam pattern of Starlink satellites is calculated and the beam switching schedule is estimated. Experimental results with received signals from six Starlink LEO satellites are presented demonstrating the beam switching strategy.

## I. INTRODUCTION

Integrated satellite-terrestrial and satellite-only broadband communication systems are currently being pursued to enhance the coverage and provide *good* wireless channel properties (Kodheli et al., 2018; Okasha et al., 2022; Judice et al., 2022; González, 2022). Due to their relatively smaller propagation delays, LEO constellations seem to be promising for latency-critical applications with requirements within tens of milliseconds. Satellite-based navigation is also witnessing the new era of low Earth orbit (LEO) *megaconstellations* (Reid et al., 2020; Kulu, 2021; Emara, 2021). The launch of tens of thousands of LEO satellites for broadband communications will revolutionize the future of satellite-based navigation (Kassas et al., 2021). The potential of utilizing LEO space vehicle (SV) signals for navigation has been the subject of numerous recent theoretical and experimental studies (Leng et al., 2016; Tan et al., 2019a,b; Elgamoudi et al., 2020; Wei et al., 2020; Farhangian and Landry, 2020; Farhangian et al., 2021; Psiaki, 2021; Nardin et al., 2021; Wang and El-Mowafy, 2022; Hartnett, 2022; Cassel et al., 2022; Khairallah and Kassas, 2021; Bilardi, 2021; Huang et al., 2022; Jiang et al., 2022; Iannucci and Humphreys, 2022; Li et al., 2022; Khairallah and Kassas, 2022; Egea-Roca et al., 2022; Zhao et al., 2022; Jardak and Jault, 2022). Broadband communication signals transmitted from LEO SVs contain timing signals, which if one could acquire and track opportunistically, navigation observables (pseudorange, carrier phase, and Doppler) could be extracted (Kozhaya and Kassas, 2022; Khalife et al., 2022).

Nevertheless, few results have been published showing experimental navigation results with real LEO SV signals. Experimental navigation results with existing LEO constellations, particularly Iridium, Orbcomm, and Globalstar for navigation, have been demonstrated in (Tan et al., 2019a; Kassas et al., 2019; Farhangian and Landry, 2020; Orabi et al., 2021; Neinavaie et al., 2021; Zhao et al., 2022). LEO megaconstellations, particularly Starlink, have attracted recent attention (Kassas et al., 2021). An opportunistic framework to navigate with differential carrier phase measurements from megaconstellation LEO SV signals was proposed in (Khalife et al., 2020), with the Starlink constellation used as a specific megaconstellation to demonstrate the efficacy of the proposed stochastic geometry-based framework. The first standalone (non-differential) positioning results with Starlink SV signals were presented in (Khalife et al., 2022; Neinavaie et al., 2022), which show carrier phase and Doppler tracking of six Starlink SVs, achieving a horizontal positioning error of 7.7 and 10 m with known receiver altitude, respectively.

The data collected during the experimental campaign for these papers suggested that the Starlink LEO satellites employed beamforming strategies as they travelled overhead. This paper attempts to unveil these beamforming strategies. To this end, based on maximum likelihood (ML) estimation of the signal to noise ratio (SNR), the beam switching schedule of real Starlink downlink signals is unveiled.

The rest of the paper is organized as follows. Section II overviews beam switching techniques of LEO satellites. Section III presents experimental results unveiling Starlink LEO satellite beamforming strategies. Section IV gives concluding remarks.

## II. BEAM SWITCHING TECHNIQUES OF LEO SATELLITES

Future applications of navigation with LEO based satellites, including differential navigation methods, may require a knowledge of beam configuration and reconfiguration in the link between the LEO SV and a ground user terminal (UT) (Del Portillo et al., 2019). Current LEO constellation device different techniques which may use some fixed analog beams that illuminate a given area of Earth's surface, or may steer narrower beams in the user's direction (Del Portillo et al., 2019). Digital precoding stages are designed independently of the analog beam aiming at minimizing the inter-beam interference between the adjacent beams (You et al., 2020). Designing a beamforming codebook at the transmitter side is crucial to guarantee coverage of the Earth's surface, limit the inter-beam interference, maximize system capacity (throughput), and exhibit compatibility with cellular standards. Recent studies on deploying LEO constellations for communication purposes do not necessarily consider the integration with terrestrial networks. For particular LEO SVs, the sizes of the beam footprints provided but the details of the beam codebook is not disclosed to public. In (Del Portillo et al., 2019; You et al., 2020), all feasible beams corresponding to a uniform planar array at the satellite are studied for massive MIMO LEO satellite communications.

### 1. Beam Codebook Design

Consider the downlink of a massive MIMO LEO satellite communication system operating in the Ku-band. A given LEO satellite in the constellation can cover an elliptical region of interest (ROI), using a set of potential beams, as illustrated in 1(a). Thus, the system supports the direct transmission to a number of simultaneous mobile user terminals (UTs) on the ground. The goal of a beam codebook design is to calculate a set of analog beam patterns or beam codebook, such that the set of beam footprints covers an ellipsoidal ROI. Depending on the location of the active users, some active beams will be selected from the set available in the codebook. A traditional precoder codebook is a discrete Fourier transform (DFT)-based analog precoder structure which can be considered as a solution for planar arrays (Palacios et al., 2021). In this case, the array response vectors in each dimension have a linearly increasing phase, like the columns in the DFT matrix. For a DFT-type codebook, the associated rectangular mesh contains some points that are covered with the same gain by multiple different satellite beams. When selecting one of the beams, the other satellites may generate interference, leading to a relatively small signal-to-interference noise ratio (SINR) as shown in Figure 1(b) (Palacios et al., 2021). Other than beamcode book, a beam switching technique is required to maximize the received SNR at a particular beam spot on the ground. In the following subsection, ML estimation of the SNR for Starlink LEO satellites is developed. Based on the estimated SNR, the beam switching schedule of Starlink satellites is unveiled.

### 2. SNR Estimation for Unknown Periodic Beacons

Similar to (Neinavaie et al., 2022), the received baseband signal is modeled as

$$r[n] = \alpha c[\tau_n - t_s[n]] \exp(j\theta[\tau_n]) + d[\tau_n - t_s[n]] \exp(j\theta[\tau_n]) + w[n], \quad (1)$$

where  $r[n]$  is the received signal at the  $n$ th time instant;  $\alpha$  is the complex channel gain between the receiver and the Starlink LEO SV;  $\tau_n$  is the sample time expressed in the receiver time;  $c[\tau_n]$  represents the samples of the complex periodic reference signal (RS) with a period of  $L$  samples;  $t_s[n]$  is the code-delay between the receiver and the Starlink LEO SV at the  $n$ th time instant;  $\theta[\tau_n] = 2\pi f_D[n]T_s n$  is the carrier phase in radians, where  $f_D[n]$  is the instantaneous Doppler frequency at the  $n$ th time instant and  $T_s$  is the sampling time;  $d_i[\tau_n]$  represents the complex samples of some data transmitted from the Starlink LEO SV; and  $w[n]$  is measurement noise, which is modeled as a complex, zero-mean, independent, and identically distributed random sequence with variance  $\sigma_w^2$ .

During the  $k$ th processing interval, the instantaneous Doppler frequency is nearly a linear function of time, i.e.,  $f_D[n] = f_{D_k} + \beta_k n$ , where  $f_{D_k}$  is referred to as constant Doppler, and  $\beta_k$  is the Doppler rate at the  $k$ th processing interval. The coherent processing interval (CPI) is defined as the time interval in which the constant Doppler,  $f_{D_k}$ , and the Doppler rate,  $\beta_k$ , are constant.

The received signal at the  $n$ th time instant when the Doppler rate is wiped-off is denoted by  $r'[n] \triangleq \exp(-j2\pi\beta_k n^2)r[n]$ . One can define *the desired RS* which is going to be detected in the acquisition stage as

$$s[n] \triangleq \alpha c[\tau_n - t_s[n]] \exp(j2\pi f_{D_k} T_s n), \quad (2)$$

and the equivalent noise as

$$w_{\text{eq}}[n] = d[\tau_n - t_s[n]] \exp(j2\pi f_{D_k} T_s n) + \exp(-j2\pi\beta n^2) w[n]. \quad (3)$$

Hence,  $r'[n] = s[n] + w_{\text{eq}}[n]$ . Due to the periodicity of the RS,  $s[n]$  has the following property

$$s[n + mL] = s[n] \exp(j\omega_k mL) \quad 0 \leq n \leq L - 1, \quad (4)$$

where  $\omega_k \triangleq 2\pi f_{D_k} T_s$  is the normalized Doppler at the  $k$ th CPI, and  $-\frac{1}{2} \leq \omega_k \leq \frac{1}{2}$ . A vector of  $L$  observation samples corresponding to the  $m$ th period of the signal is formed as

$$\mathbf{z}_m \triangleq [r'[mL], r'[mL+1], \dots, r'[(m+1)L-1]]^T. \quad (5)$$

The  $k$ th CPI vector is constructed by concatenating  $M$  vectors of length  $L$  to form the  $ML \times 1$  vector

$$\mathbf{y}_k = [\mathbf{z}_{kM}^T, \mathbf{z}_{kM+1}^T, \dots, \mathbf{z}_{(k+1)M-1}^T]^T. \quad (6)$$

Therefore,

$$\mathbf{y}_k = \mathbf{H}_k \mathbf{s} + \mathbf{w}_{\text{eq}k}, \quad (7)$$

where  $\mathbf{s} = [s[1], s[2], \dots, s[L]]^T$ , and the  $ML \times L$  Doppler matrix is defined as

$$\mathbf{H}_k \triangleq [\mathbf{I}_L, \exp(j\omega_k L) \mathbf{I}_L, \dots, \exp(j\omega_k (M-1)L) \mathbf{I}_L]^T, \quad (8)$$

where  $\mathbf{I}_L$  is an  $L \times L$  identity matrix and  $\mathbf{w}_{\text{eq}k}$  is the equivalent noise vector. Assuming that the index of the first CPI is  $k = 0$ , for a given set of unknown variables  $\mathcal{W}_0 = \{L, \omega_0, \beta_0\}$ , the ML estimation of the SNR is (see Theorem 9.1 in (Kay, 1993))

$$\widehat{\text{SNR}}(\mathbf{y}_0 | \mathcal{W}_0) = \frac{\mathbf{y}_0^H \mathbf{P}_{\mathbf{H}_0} \mathbf{y}_0}{\mathbf{y}_0^H \mathbf{P}_{\mathbf{H}_0}^\perp \mathbf{y}_0}, \quad (9)$$

where  $\mathbf{y}_0^H$  is the Hermitian transpose of  $\mathbf{y}_0$ ,  $\mathbf{P}_{\mathbf{H}_0} \triangleq \mathbf{H}_0 (\mathbf{H}_0^H \mathbf{H}_0)^{-1} \mathbf{H}_0^H$  denotes the projection matrix to the column space of  $\mathbf{H}_0$ ,  $\mathbf{P}_{\mathbf{H}_0}^\perp \triangleq \mathbf{I} - \mathbf{P}_{\mathbf{H}_0}$  denotes the projection matrix onto the space orthogonal to the column space of  $\mathbf{H}_0$ , and the ML estimate of  $\mathcal{W}_0$  is (Neinavaie et al., 2022)

$$\hat{\mathcal{W}}_0 = \underset{L, \omega_0, \beta_0}{\text{argmax}} \|\mathbf{H}_0^H \mathbf{y}_0\|^2. \quad (10)$$

As it can be seen in Figure 2, due to the high dynamics of the satellite, different beams should be selected to illuminate a beam spot on the ground as the satellite moves.

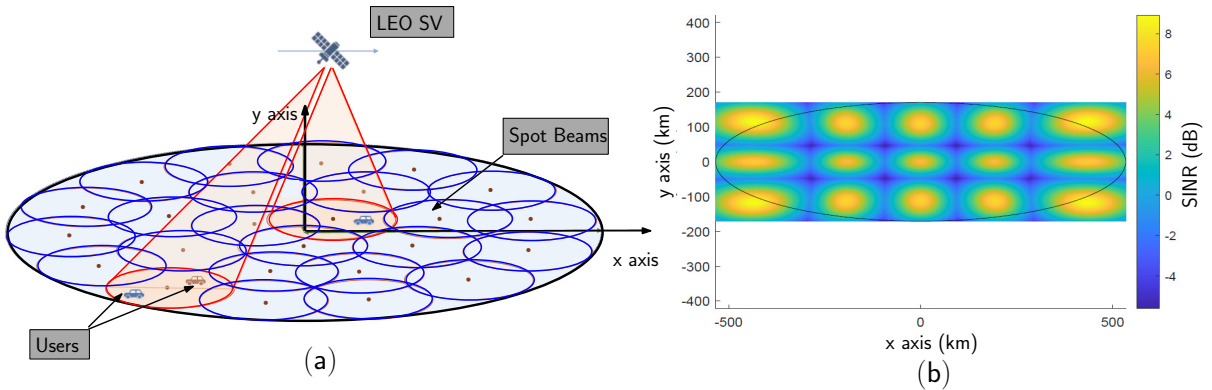


**Figure 1:** (a) A LEO satellite communication system covering an elliptical area using a predefined beam codebook. (b) Rectangular mesh covering the elliptical ROI when using the oversampled DFT beam and SINR when using the beam with maximum power for each cell.

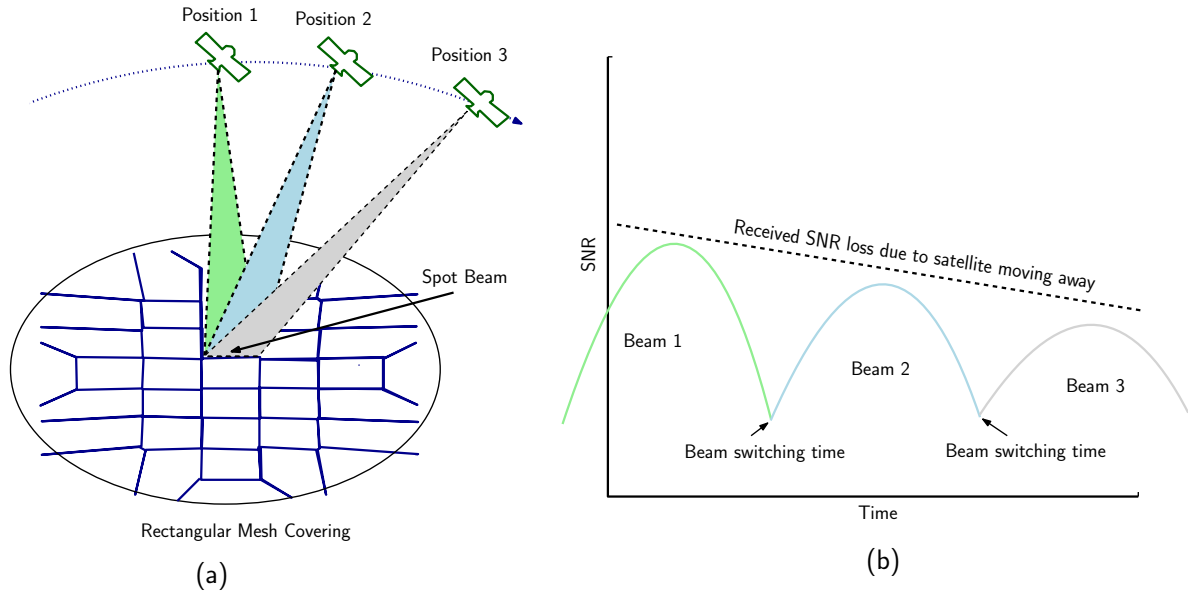


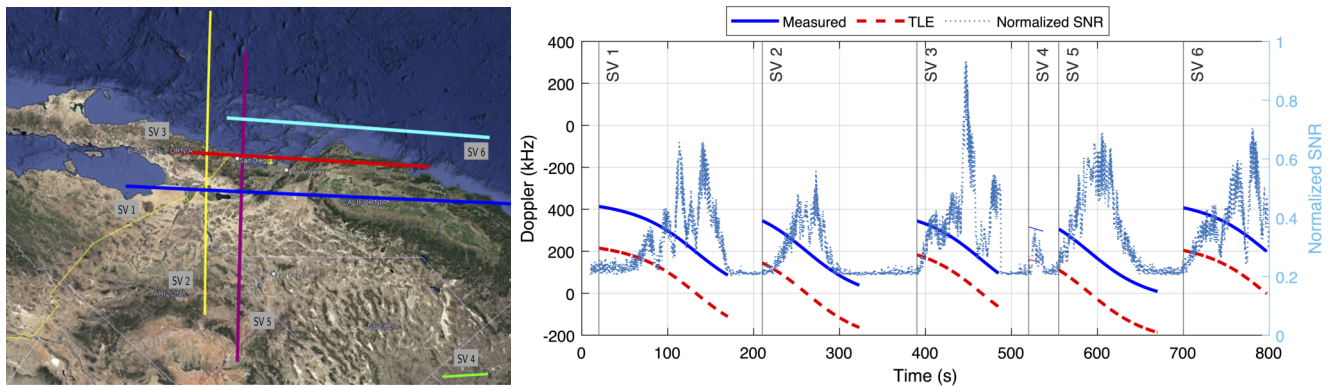
**Figure 2:** The beam switching configuration of LEO satellites based on SNR maximization at the spot beam: (a) Rectangular mesh covering of the ground surface and different beams illuminating the spot beam (b) The reduction of the receive SNR at the spot beam due to satellite moving away and beam switching times.

### III. STARLINK BEAMFORMING STRATEGIES

This section presents an experimental demonstration of Starlink’s beamforming strategies. The provided information allows for designing navigation techniques that benefit from differential measurements from multiple users that see the same satellite. To guarantee that two users with a given baseline can receive signals from the same satellite, some information about beamforming configurations should be available about these satellites.

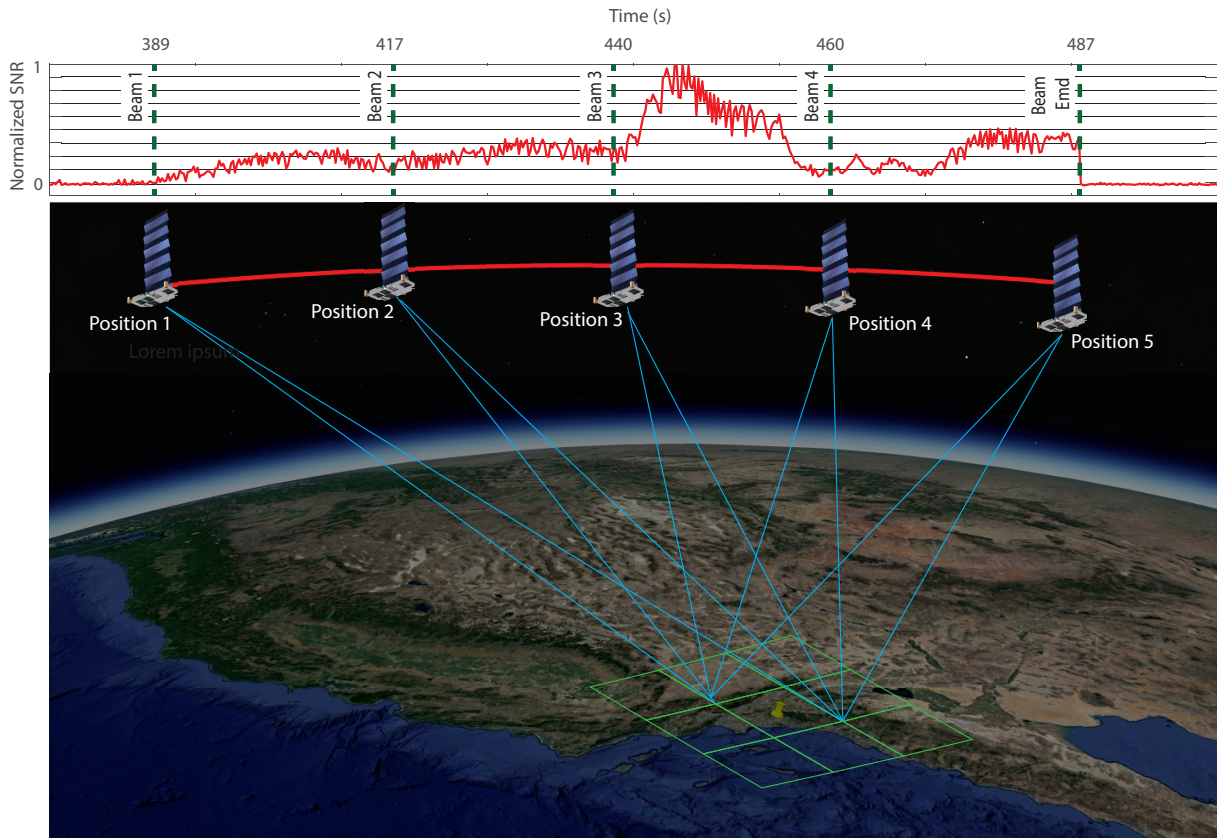
The experimental setup used consisted of a stationary National Instrument (NI) universal software radio peripheral (USRP) 2945R was equipped with a consumergrade Ku antenna and low-noise block (LNB) downconverter to receive Starlink signals in the Ku-band. The sampling rate was set to 2.5 MHz and the carrier frequency was set to 11.325 GHz, which is one of the Starlink downlink frequencies.

Figure 3 demonstrates the estimated Doppler, the normalized SNRs, and the skyplot for six Starlink satellites passes. For each satellite, multiple peaks can be observed, as expected, with each peak corresponding to a beam. The increasing and decreasing behavior of the peaks indicates whether the satellite is approaching or moving away. Also, the effect of beam switching to maintain maximum SNR can be observed in the estimated receive SNRs. The maximum received SNR is achieved when Starlink LEO SV 3 is passing above the receiver.



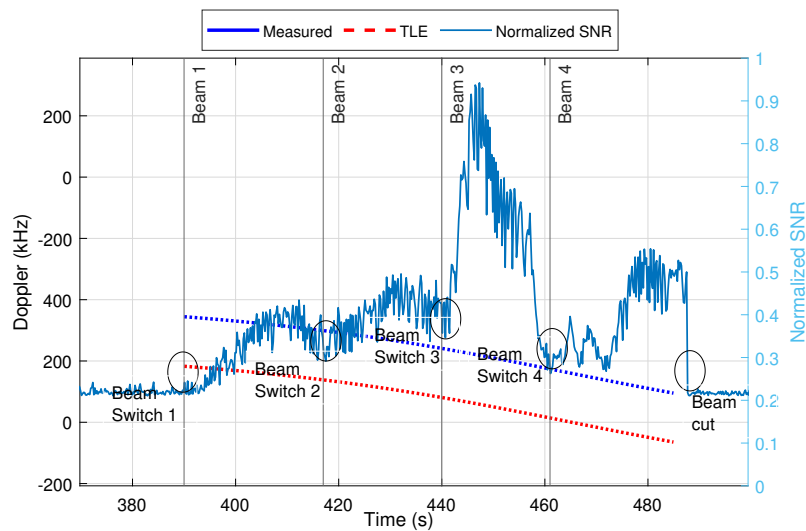
**Figure 3:** Estimated SNRs and Doppler frequencies of six Starlink satellites: Each satellite illuminates the spot beam of interest with different beams. The maximum SNR occurs when SV 3 is passing above the receiver.

Figure 4, shows the Starlink LEO SVs trajectory and the locations in which the beam is taken place. It can also be seen that the satellite stops illuminating the region at a particular time instant.



**Figure 4:** Sky plot of the Starlink SV3 and the beam switch schedule for the spot beam of interest: (a) The satellite’s trajectory and the time instants at which the beam is switched is demonstrated which shows that the spot beam is illuminated around 30 seconds by each beam.

Figure 5 shows the SNR change of Starlink LEO SV 3 corresponding to different beams illuminating the spot beam at which the receiver is located.



**Figure 5:** The receive SNR corresponding to Starlink SV 3 shows that the satellite is approaching around  $t = 450$  s and moving away from this time instant. It is also observed that the beam is ended at around  $t = 490$  s.

## IV. CONCLUSION

This paper studied the beamforming strategies of Starlink LEO satellites. Using ML estimation of the SNR, the beam switching schedule of Starlink satellites was studied and demonstrated experimentally.

## ACKNOWLEDGEMENTS

This work was supported in part by the Office of Naval Research (ONR) under N00014-19-1-2511 and Grant N00014-22-1-2242.

## REFERENCES

- Bilardi, S. (2021). A gnss signal simulator and processor for evaluating acquisition and tracking of GPS-like signals from satellites in LEO. Master's thesis, University of Colorado at Boulder, CO, USA.
- Cassel, R., Scherer, D., Wilburne, D., Hirschauer, J., and Burke, J. (2022). Impact of improved oscillator stability on LEO-based satellite navigation. In *Proceedings of ION International Technical Meeting*, pages 893–905.
- Del Portillo, I., Cameron, B., and Crawley, E. (2019). A technical comparison of three low earth orbit satellite constellation systems to provide global broadband. *Acta Astronautica*, 159:123–135.
- Egea-Roca, D., Lopez-Salcedo, J., Seco-Granados, G., and Falletti, E. (2022). Performance analysis of a multi-slope chirp spread spectrum signal for PNT in a LEO constellation. In *Proceedings of Workshop on Satellite Navigation Technology*, pages 1–9.
- Elgamoudi, A., Benzerrouk, H., Elango, G., and Landry, R. (2020). Gauss Hermite  $h_\infty$  filter for UAV tracking using LEO satellites TDOA/FDOA measurementpart I. *IEEE Access*, 8:201428–201440.
- Emara, S. (2021). Positioning in non-terrestrial networks. Master's thesis, Lund University, Sweden.
- Farhangian, F., Benzerrouk, H., and Landry, R. (2021). Opportunistic in-flight INS alignment using LEO satellites and a rotatory IMU platform. *Aerospace*, 8(10):280–281.
- Farhangian, F. and Landry, R. (2020). Multi-constellation software-defined receiver for Doppler positioning with LEO satellites. *Sensors*, 20(20):5866–5883.
- González, T. (2022). Channel modeling in IOT deployments supported by LEO nanosatellites. Master's thesis, Universidad de Chile.
- Hartnett, M. (2022). Performance assessment of navigation using carrier Doppler measurements from multiple LEO constellations. Master's thesis, Air Force Institute of Technology, Wright-Patterson Air Force Base, Ohio, USA.
- Huang, C., Qin, H., Zhao, C., and Liang, H. (2022). Phase - time method: Accurate Doppler measurement for Iridium NEXT signals. *IEEE Transactions on Aerospace and Electronic Systems*, pages 1–9.
- Iannucci, P. and Humphreys, T. (2022). Fused low-Earth-orbit GNSS. *IEEE Transactions on Aerospace and Electronics Systems*. accepted.
- Jardak, N. and Jault, Q. (2022). The potential of LEO satellite-based opportunistic navigation for high dynamic applications. *Sensors*, 22(7):2541–2565.
- Jiang, M., Qin, H., Zhao, C., and Sun, G. (2022). LEO Doppler-aided GNSS position estimation. *GPS Solutions*, 26(1):1–18.
- Judice, A., Venusamy, K., and Livin, J. (2022). Multilayer LEO satellite constellation coverage analysis and its current research directions. In *Proceedings of IEEE International Conference on Distributed Computing and Electrical Circuits and Electronics*, pages 1–5.
- Kassas, Z., Morales, J., and Khalife, J. (2019). New-age satellite-based navigation – STAN: simultaneous tracking and navigation with LEO satellite signals. *Inside GNSS Magazine*, 14(4):56–65.
- Kassas, Z., Neinaiaie, M., Khalife, J., Khairallah, N., Haidar-Ahmad, J., Kozhaya, S., and Shadram, Z. (2021). Enter LEO on the GNSS stage: Navigation with Starlink satellites. *Inside GNSS Magazine*, 16(6):42–51.
- Kay, S. (1993). *Fundamentals of statistical signal processing: Detection Theory*, volume II. Prentice-Hall, Upper Saddle River, NJ.
- Khairallah, N. and Kassas, Z. (2021). Ephemeris closed-loop tracking of LEO satellites with pseudorange and Doppler measurements. In *Proceedings of ION GNSS Conference*, pages 2544–2555.

- Khairallah, N. and Kassas, Z. (2022). An interacting multiple model estimator of LEO satellite clocks for improved positioning. In *Proceedings of IEEE Vehicular Technology Conference*, pages 1–5.
- Khalife, J., Neinavaie, M., and Kassas, Z. (2020). Navigation with differential carrier phase measurements from megaconstellation LEO satellites. In *Proceedings of IEEE/ION Position, Location, and Navigation Symposium*, pages 1393–1404.
- Khalife, J., Neinavaie, M., and Kassas, Z. (2022). The first carrier phase tracking and positioning results with Starlink LEO satellite signals. *IEEE Transactions on Aerospace and Electronic Systems*, 56(2):1487–1491.
- Kodheli, O., Guidotti, A., and Vanelli-Coralli, A. (2018). Integration of satellites in 5G through LEO constellations. In *Proceedings of the IEEE Global Communications Conference*, pages 1–6.
- Kozhaya, S. and Kassas, Z. (2022). Blind receiver for LEO beacon estimation with application to UAV carrier phase differential navigation. In *Proceedings of ION GNSS Conference*. accepted.
- Kulu, E. (2021). Satellite constellations–2021 industry survey and trends. In *Proceedings of Annual Small Satellite Conference*, pages 1–20.
- Leng, M., Quitin, F., Tay, W., Cheng, C., Razul, S., and See, C. (2016). Anchor-aided joint localization and synchronization using SOOP: Theory and experiments. *IEEE Transactions on Wireless Communications*, 15(11):7670–7685.
- Li, M., Xu, T., Guan, M., Gao, F., and Jiang, N. (2022). LEO-constellation-augmented multi-GNSS real-time PPP for rapid re-convergence in harsh environments. *GPS Solutions*, 26(1):1–12.
- Nardin, A., Dovis, F., and Fraire, J. (2021). Empowering the tracking performance of LEO-based positioning by means of meta-signals. *IEEE Journal of Radio Frequency Identification*, 5(3):244–253.
- Neinavaie, M., Khalife, J., and Kassas, Z. (2021). Doppler stretch estimation with application to tracking Globalstar satellite signals. In *Proceedings of IEEE Military Communications Conference*, pages 647–651.
- Neinavaie, M., Khalife, J., and Kassas, Z. (2022). Acquisition, Doppler tracking, and positioning with Starlink LEO satellites: First results. *IEEE Transactions on Aerospace and Electronic Systems*, 58(3):2606–2610.
- Okasha, N., Zekry, A., and Newagy, F. (2022). Hybrid VLC vehicle to vehicle and LEO satellite communication system for highway road coverage. In *Proceedings of International Conference on Computing, Control and Industrial Engineering*, pages 571–583.
- Orabi, M., Khalife, J., and Kassas, Z. (2021). Opportunistic navigation with Doppler measurements from Iridium Next and Orbcomm LEO satellites. In *Proceedings of IEEE Aerospace Conference*, pages 1–9.
- Palacios, J., Gonzalez-Prelcic, N., Mosquera, C., Shimizu, T., and Wang, C. (2021). A hybrid beamforming design for massive MIMO LEO satellite communications. *arXiv preprint arXiv:2104.11158*.
- Psiaki, M. (2021). Navigation using carrier Doppler shift from a LEO constellation: TRANSIT on steroids. *NAVIGATION, Journal of the Institute of Navigation*, 68(3):621–641.
- Reid, T., Chan, B., Goel, A., Gunning, K., Manning, B., Martin, J., Neish, A., Perkins, A., and Tarantino, P. (2020). Satellite navigation for the age of autonomy. In *Proceedings of IEEE/ION Position, Location and Navigation Symposium*, pages 342–352.
- Tan, Z., Qin, H., Cong, L., and Zhao, C. (2019a). New method for positioning using IRIDIUM satellite signals of opportunity. *IEEE Access*, 7:83412–83423.
- Tan, Z., Qin, H., Cong, L., and Zhao, C. (2019b). Positioning using IRIDIUM satellite signals of opportunity in weak signal environment. *Electronics*, 9(1):37.
- Wang, K. and El-Mowafy, A. (2022). LEO satellite clock analysis and prediction for positioning applications. *Geo-spatial Information Science*, 25(1):14–33.
- Wei, Q., Chen, X., and Zhan, Y. (2020). Exploring implicit pilots for precise estimation of LEO satellite downlink Doppler frequency. *IEEE Communications Letters*, 24(10):2270–2274.
- You, L., Li, K., Wang, J., Gao, X., Xia, X., and Ottersten, B. (2020). Massive MIMO transmission for LEO satellite communications. <https://arxiv.org/pdf/2002.08148.pdf>.
- Zhao, C., Qin, H., and Li, Z. (2022). Doppler measurements from multiconstellations in opportunistic navigation. *IEEE Transactions on Instrumentation and Measurement*, 71:1–9.